Chemical Communications

Communication

Controlled fabrication of osmium nanocrystals by electron, laser and microwave irradiation and characterisation by microfocus X-ray absorption spectroscopy

Anaïs Pitto-Barry,[a,b] Kalotina Geraki,[c] Michael D. Horbury,[a] Vasilios G. Stavros,[a] J. Frederick W. Mosselmans,[c] Richard I. Walton,[a] Peter J. Sadler,*[a] and Nicolas P. E. Barry*[a,b]

Received (in XXX, XXX) Xth XXXXXXXXX 20XX, Accepted Xth XXXXXXXXX 20XX

Osmium nanocrystals can be fabricated by electron (3-50 nm, formed by atom migration), 785-815 nm laser (20-50 nm, in micelle islands), and microwave (*ca.* 1 nm in arrays, > 100 mg scale) irradiation of a polymer-encapsulated Os^{II} carborane; microfocus X-ray absorption studies at the Os L_{III}-edge show differences between the three preparation methods, suggesting that the electron-beam irradiated materials have a significant support interaction and/or surface oxidation, while the laser and microwave samples are more like metallic osmium.

The third-row transition element osmium, a precious metal, is the densest of all elements (22.58 g/cm^3, ambient conditions).[1] It has the highest melting point (3306 K) and lowest vapour pressure of the platinum group metals (Ru, Rh, Pd, Os, Ir, Pt).[2] Osmium nanocrystals offer considerable potential for a range of applications in the development of pressure-resistant, highly dense, nanomaterials.[3-7] Their dimensions (1 – 100 nm) are likely to result in physical and chemical properties that differ significantly from those of bulk osmium,[8] but have yet to be explored.

We recently introduced a general method for fabrication of boron- and sulfur/selenium-doped-graphitic matrices decorated with very small, 3D-metal nanocrystals of defined size.[9-12] We irradiated boron-rich precious metal-encapsulated self-spreading polymer micelles with electrons in a transmission electron microscope (TEM) chamber under vacuum, and produced a doped graphitic support on which individual osmium atoms hop and migrate to form 3D-nanocrystals, as small as 15 Å in diameter within 1 hour. This technology allowed experimental observation of nanocrystal assembly from single metal atoms and captured the dynamics of single atom motion and metal cluster formation in real space with atomic precision.[9] Here, we report an important advance in the methodology for the fabrication of osmium nanocrystals by irradiating metal-encapsulated self-spreading polymer micelles with a laser beam or with microwave irradiation. These new procedures will allow the fabrication of nanocrystals on a much larger scale than in the TEM. We have used microfocus X-ray absorption spectroscopy (XAS) at the Os L_{III}-edge to characterise the nanocrystals formed by these different methodologies (electron beam, laser, and microwave irradiation), by studying crystals deposited on TEM grids. This has allowed heterogeneity in different regions on the grids to be examined and structural information to be quantified.

Nanometre-sized Os nanocrystals were first prepared by electron-beam irradiation *via* TEM on 400-mesh lacey-carbon gold grids (**G1**), as hundreds of nanocrystals per 100 nm^2 spread over the 3 × 3 mm^2 grid, in accordance with our previously reported methodology.[11] This procedure involves the encapsulation of the organometallic half-sandwich Os^{II} arene complex [Os(*p*-cymene)(1,2-dicarba-*closo*-dodecarborane-1,2-dithiolate)] (**1**), a 16-electron complex[13] which is highly hydrophobic[14] in the water-soluble amphiphilic triblock copolymer P123[15] at ambient temperature for 4 h, to form osmium-containing micelles (**OsMs**). A drop of sample (5 μL – 1 mg/mL of micelles) was then deposited on the grid and left to air-dry. The grids were subsequently irradiated by the defocused electron beam of a TEM (irradiation of the whole grid) for 12 h to produce Os nanocrystals of *ca.* 3 nm of diameter. The mechanism of degradation by TEM most likely arises from reduction of Os(II) to Os(0) owing to the flux of electrons, and the kinetic energy of the electron beam is probably the main driving force for the dynamic behaviour of the metal atoms observed in TEM, but the precise mechanism of the degradation is still under investigation and requires further work. The movement of energised nanoclusters themselves, induced by the electron beam, results in contact with neighbouring particles, and eventual merging and coalescence.[9]

We then investigated new methodologies for the fabrication of Os nanocrystals. Solutions of **OsMs** were deposited on lacey carbon 400 mesh gold TEM grids (**G2**) as described above. The grids were irradiated for 5 h using a laser wavelength of 785-815 nm with an average power of 33 mW to produce Os nanocrystals. The grids were examined with a high-resolution TEM (HRTEM, 80 keV; 1.9 pA/cm^2; irradiated area *ca.* 200×200 nm^2; Figure 1) as briefly as possible (less than 1 min of irradiation of minimal brightness) in order to avoid electron beam-induced formation of nanocrystals. Electron-beam irradiation under these TEM conditions would be expected to give rise to nanocrystals in *ca.* 20 min.[9] Remarkably, it was apparent that islands of nanocrystals were produced over the whole grid by the laser irradiation (Figure 1), rather than the observed more widely spread nanocrystals fabricated by the electron beam,[11] suggesting that the mechanism of formation of the nanocrystals in the laser beam is distinct from

that of electron beam irradiation. Interestingly, the size of the islands made up of nanocrystals ranged from 20 to 50 nm, close to the diameter of the **OsMs** micelles containing the metal complex before irradiation.[16] This suggests that the degradation of the micelles induced by the laser is either very fast, which leads to decoordination of the ligands and formation of metal-metal bonds, or that the polymer matrix is less affected by the laser than by the electron beam, therefore reducing the mobility of metallic atoms,[12] and facilitating formation of nanocrystals in close vicinity.

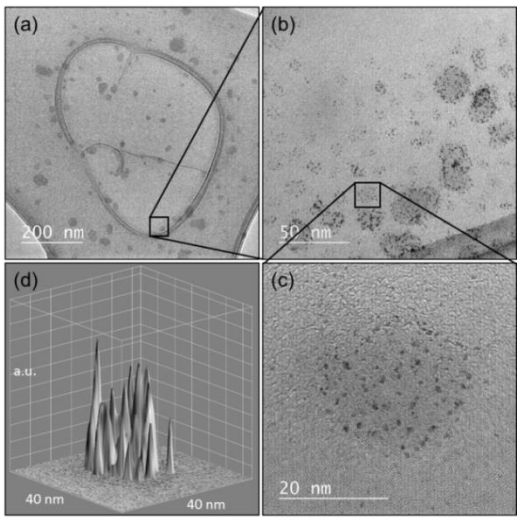

Fig. 1 (a-c) HRTEM images at 3 different magnifications of Os nanocrystals on lacey carbon TEM grids made by laser irradiation. The islands of nanocrystals have similar sizes to the precursor polymer micelles.[16] (d) 3D projection of the area shown in (c) highlighting the difference of contrast between Os nanocrystals and the background.

We then attempted to produce the Os nanocrystals *via* microwave-assisted synthesis. 100 mg of freeze-dried **OsMs** were heated at 190 °C for 8 min at 250 psi in a sealed vessel. The residue was dissolved in water, and a drop of sample (5 μL, 1 mg/mL) was deposited on a TEM grid and left to air-dry for examination by high-resolution TEM (**G3**). As with the laser methodology, the TEM images were recorded as quickly as possible (less than 1 min with minimal brightness) to avoid the production of nanocrystals by electron irradiation. Arrays of very small nanocrystals of *ca.* 1 nm were readily observable across the whole surface of the grid (Figure 2). Microwave/laser irradiation may lead to the bond cleavage and production of radicals[17] that might be the source of the electrons which reduce Os(II) to Os(0). To investigate the effect of the electron beam on the nanocrystals, the grid was exposed for a further 10 min. Interestingly, a rapid degradation of the underlying surface was observed (in < 10 min), which is much faster than without pre-microwave irradiation at this electron flux. In the electron beam alone such degradation takes up to 80 min.[9] It is notable that the size distribution of the nanocrystals produced by the three methods is remarkably similar (see Figure S1). An advantage of using microwave irradiation for the fabrication of nanoparticles is that it allows fabrication on a larger scale than by electron irradiation in a TEM chamber. Several hundreds of milligrams of micelle precursors can be irradiated within 10 min offering the possibility to measure bulk properties from the samples. For example, infrared spectroscopy clearly showed the disappearance of the characteristic carborane B−H stretching vibration band at 2550 cm^{-1} after microwave treatment of the **OsMs** micelles (Figure S2).

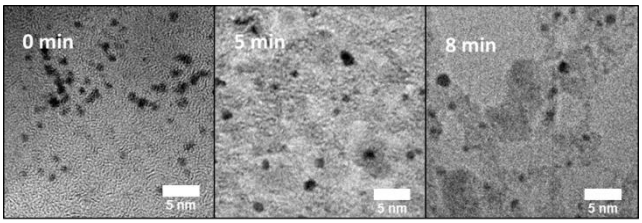

Fig. 2 HRTEM images of Os nanocrystals fabricated by microwave-assisted synthesis in aqueous solution (1 mg/mL of **OsMs** precursors). All the images are from the same area and show the degradation of the underlying surface upon electron beam irradiation.

Samples of nanocrystals produced by electron (**G1**), laser (**G2**) or microwave (**G3**) irradiation were prepared on lacey carbon gold TEM grids. The choice of gold as grid material was to avoid interference from the X-ray fluorescence of copper, more commonly used for grids. Since the amount of crystals on the various TEM grids was very small (5 μL of a 1 mg/mL solution of precursor deposited; 7.14 picomol of Os metal), we explored the use of microfocus XAS to examine various regions of the TEM grids, using the X-ray absorption near edge structure (XANES) to investigate the oxidation state and extended X-ray absorption fine structure (EXAFS) at the Os L_{III}-edge for nearest neighbour structural information. Fluorescence mode was used for the grids and transmission mode for Os standards, at ambient temperature on beamline I18[18] of the Diamond Light Source. A 5 × 5 μm^2 beam was used for the microXAS data collection in fluorescence mode, while the beam size was increased to 30 × 30 μm^2 to collect the transmission data The edge calibration standards were three samples of different oxidation states in cellulose pellets: **S0**: Os(0) - osmium powder; **S1**: Os(II) – $[(\eta^6\text{-}p\text{-cym})Os(\mu\text{-Cl})Cl]_2$; and **S2**: Os(IV) - sodium osmium hexachloroosmate dihydrate (Figure 3a, and Table S1). We used the position of the white line (*i.e.* absorption maximum) as a measure of edge shift and the calibration is in accordance with previous Os L_{III}-edge XAS studies,[19-21] with a shift of ~0.5 eV per oxidation state unit. The spectra of two known Os(II) complexes (**1** and [Os(*p*-cymene)(1,2-dicarba-*closo*-dodecarborane-1,2-dithiolate)(triphenylphosphine)] **2**) were also recorded as pellets in transmission mode, in order to test the reproducibility of the calibration curve and the stability of these complexes towards the X-ray beam (Figure 3b).

The low edge energy for complex **1** (calculated oxidation state ~0), suggests a reduction and degradation of the compound in the X-ray beam to osmium metal, but for complex **2** is close to the expected oxidation state of +2, showing its greater stability towards the X-ray beam. The samples on the grids show stability in the X-ray beam and although measurements on different regions of each of these grids reveal some heterogeneity in average Os oxidation state, it is noteworthy that there are systematic differences between the grids prepared by each method (Figure 3b). The sample prepared by electron beam irradiation always showed a higher Os oxidation state (+1.9 on average), while only the microwave sample showed an oxidation

state closes to 0; the laser sample showing an intermediate oxidation state.

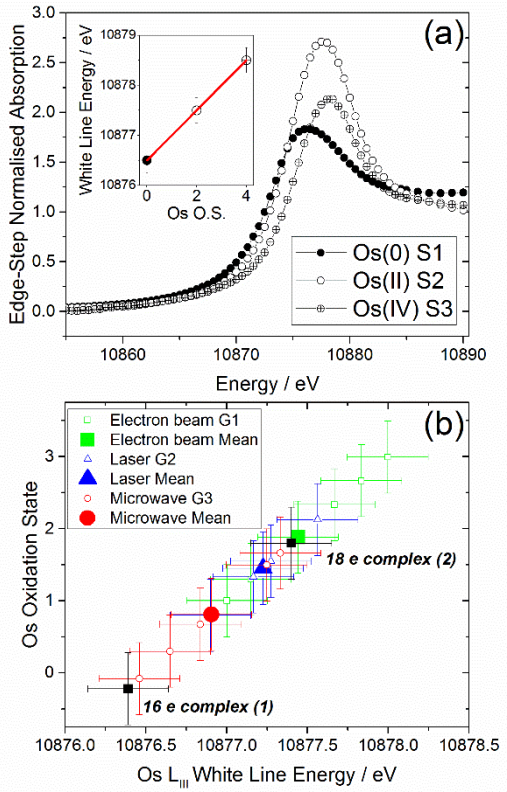

Fig. 3 (a) Os L_{III}-edge XANES from reference materials with oxidation state *versus* Os L_{III}-edge edge energy calibration curve shown as the inset. (b) Edge positions and calculated Os oxidation states for complexes **1** and **2** (black squares), from different regions of each of the three grids (open symbols), with mean values shown by the large closed symbols.

In an attempt to quantify the coordination environments of the Os atoms in the nanocrystals, EXAFS data for the organometallic half-sandwich Os^{II} arene complex **1** were first collected in transmission mode. The data (Table S2) were best fitted as Os metal (Figure 4a), which is consistent with the instability of this complex, the complex used to prepare the Os nanoclusters by irradiation: presumably the high intensity and/or energy of the X-ray beam causes decomposition.

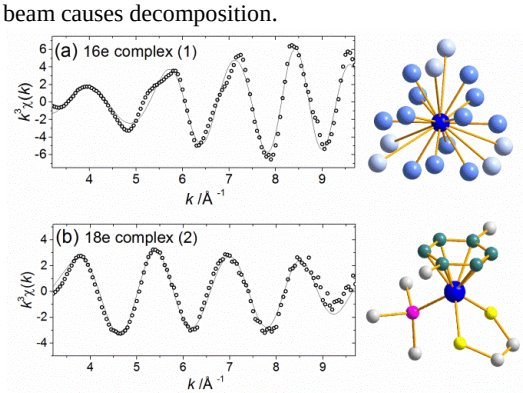

Fig. 4 k^3-weighted Os L_{III}-edge EXAFS of (a) complex **1** and (b) complex **2**. The structures are the clusters fitted to the data points: for **1** metallic osmium with two shells of atoms indicated by different shades of blue and for **2** the crystal structure of the Ru analogue of the complex (see Table S2 for fitted parameters).

To verify the feasibility of characterising carborane-containing half-sandwich complexes by EXAFS analysis, the more electronically stable triphenylphosphine (PPh_3) complex **2** was prepared and measured in transmission mode. This complex was chosen owing to its stability under irradiation (no degradation and formation of nanoclusters was observed by electron beam irradiation). In this case, the fitting of the Os L_{III} EXAFS data leads to the determination of the expected first and second coordination shells (although the S and P shells are too close to be distinguished and the atomic numbers of S and P are similar, so these were modelled as a single shell of 3 S atoms; Figure 4b).

EXAFS data for the nanocrystals prepared by laser, microwave and electron beam irradiation methods were then analysed (Figure 5). The data from sample **G2** prepared by laser irradiation were fitted to the Os metal model, with a reasonable fit (Figure 5b), consistent with the XANES analysis described above. The microwave-prepared sample **G3**, expected to have on average a slightly higher Os oxidation state, can also be fitted reasonably well as metallic osmium, which suggests that the amount of secondary material is small. In contrast the data from the electron-beam irradiated sample **G1** are not well fitted by the osmium metal model, and to achieve a satisfactory fit a further shell of sulfur atoms was included (Figure 5a). This is consistent with the XANES results that shows the highest average oxidation state for Os out of the three grids, and might be interpreted as osmium metal particles with a terminating shell of sulfur atoms, for example from the support. Although a mixture of phases cannot be ruled out by the EXAFS method which detects an average of all atomic environments, it is important to note that **G1** cannot contain undecomposed precursor complex (**1**), since as we showed above, this complex spontaneously decomposes in the X-ray beam.

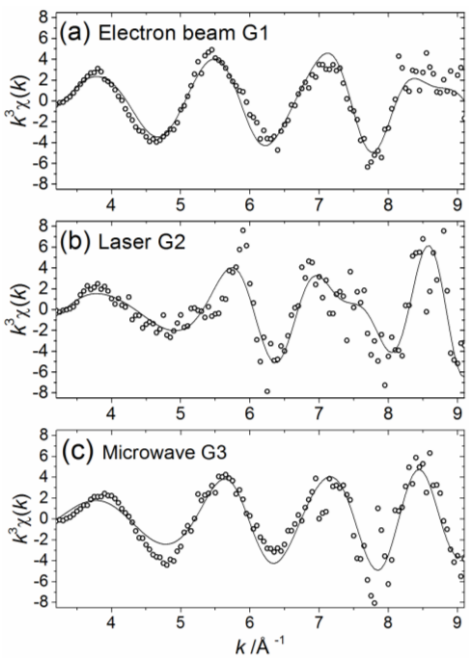

Fig. 5 k^3-weighted Os L_{III}-edge EXAFS of grids prepared using (a) electron-bean irradiation (b) laser and (c) microwave irradiation.

We have shown that laser and microwave irradiation of a polymer-encapsulated osmium dithiocarborane complex can

produce osmium nanocrystals. These methods offer potential advantages over our previously reported high energy electron irradiation method, including convenience of more readily available equipment and possible scale-up of production. Whilst the TEM allow the fabrication of crystals only at the pico-gram scale, hundreds of milligrams of nanocrystals can be synthesised via both microwave and laser procedures. Although technically challenging, recent advances in design of X-ray synchrotron beam focussing now allow XAS data to be collected from TEM grids at micrometre level of resolution. Laser irradiation produced arrays of nanocrystals in localised areas of the sizes of the micelle precursors,[16] whilst the microwave-assisted fabrication of nanocrystals led to arrays of very small nanocrystals of *ca*. 1 nm across covering the all the surface of the grids (as for electron beam irradiation), but with rapid degradation of the underlying surface under the electron beam, a phenomenon which is observed only after more than 1 h when the crystals are produced by electron irradiation. The XAS data suggest that these osmium nanocrystals contain a mixture of oxidation states, not merely Os^0 atoms as appeared to be the case from TEM imaging. It seems clear that surface Os atoms are reactive and readily oxidised, as deduced also from X-ray photoelectron spectroscopic data.[11] The stability of the osmium nanocrystals, when imaged in the X-ray beam after fabrication, depended on the fabrication method and probably reflects the nature of the supporting matrix. Our experiments suggest a wide range of future experiments which may open up new areas of application such as nanocatalysis, *e.g.* the effect of exposure of the nanocrystals to O_2 and other gases such as CO and H_2 together with appropriate substrates. This will require use of a chamber in which nanocrystals produced under controlled conditions by electron, microwave or laser treatment of precursor complexes can be transferred to the synchrotron beamline without uncontrolled exposure to air. Similar experiments on other precious metals such as Rh, Ir, Pd, Pt and Au will also be feasible.

Acknowledgments

We thank the Royal Society (University Research Fellowship No. UF150295 to NPEB), the Leverhulme Trust (Early Career Fellowship No. ECF-2013-414 to NPEB), the ERC (Grant No. 247450 to PJS), EPSRC (Grant No. EP/F034210/1 to PJS and EP/J007153/1 to VGS), Diamond Light Source (Beam-time grant number SP11314). We also thank Alexander Dunn for assistance with the data collection and some preliminary data analysis.

Notes and references

a) Department of Chemistry, University of Warwick, Coventry CV4 7AL, United Kingdom.
b) School of Chemistry and Biosciences, University of Bradford, Bradford BD7 1DP
c) Diamond Light Source Ltd, Diamond House, Harwell Campus, Didcot OX11 0DE
Tel: +44 (0)127423 6144; N.Barry@bradford.ac.uk; P.J.Sadler@warwick.ac.uk

1. *CRC Handbook of Chemistry and Physics*, CRC Press, 92nd Edition, 2011.
2. G. W. C. Kaye and T. H. Laby, in *Tables of Physical and Chemical Constants*, Longman, 16th Edition, 1995.
3. E.-K. Lim, T. Kim, S. Paik, S. Haam, Y.-M. Huh and K. Lee, *Chem. Rev.*, 2014, DOI: 10.1021/cr300213b.
4. J. Yao, M. Yang and Y. Duan, *Chem. Rev.*, 2014, **114**, 6130-6178.
5. J. A. Hubbell and A. Chilkoti, *Science*, 2012, **337**, 303-305.
6. D. Jariwala, V. K. Sangwan, L. J. Lauhon, T. J. Marks and M. C. Hersam, *Chem. Soc. Rev.*, 2013, **42**, 2824-2860.
7. B. Cornelio, G. A. Rance, M. Laronze-Cochard, A. Fontana, J. Sapi and A. N. Khlobystov, *J. Mater. Chem. A*, 2013, **1**, 8737-8744.
8. J. Jortner and C. N. R. Rao, *Pure Appl. Chem.*, 2002, **74**, 1491-1506.
9. N. P. E. Barry, A. Pitto-Barry, A. M. Sanchez, A. P. Dove, R. J. Procter, J. J. Soldevila-Barreda, N. Kirby, I. Hands-Portman, C. J. Smith, R. K. O'Reilly, R. Beanland and P. J. Sadler, *Nat. Commun.*, 2014, **5**, 3851.
10. A. Pitto-Barry, P. J. Sadler and N. P. E. Barry, *Chem. Commun.*, 2016, **52**, 3895-3898.
11. A. Pitto-Barry, L. M. A. Perdigao, M. Walker, J. Lawrence, G. Costantini, P. J. Sadler and N. P. E. Barry, *Dalton Trans.*, 2015, **44**, 20308-20311.
12. N. P. E. Barry, A. Pitto-Barry, J. Tran, S. E. F. Spencer, A. M. Johansen, A. M. Sanchez, A. P. Dove, R. K. O'Reilly, R. J. Deeth, R. Beanland and P. J. Sadler, *Chem. Mater.*, 2015, **27**, 5100-5105.
13. M. Herberhold, H. Yan and W. Milius, *J. Organomet. Chem.*, 2000, **598**, 142-149.
14. M. Scholz and E. Hey-Hawkins, *Chem. Rev.*, 2011, **111**, 7035-7062.
15. A. Pitto-Barry and N. P. E. Barry, *Polym. Chem.*, 2014, **5**, 3291-3297.
16. N. P. E. Barry, A. Pitto-Barry, I. Romero-Canelon, J. Tran, J. J. Soldevila-Barreda, I. Hands-Portman, C. J. Smith, N. Kirby, A. P. Dove, R. K. O'Reilly and P. J. Sadler, *Faraday Discuss.*, 2014, **175**, 229-240.
17. C. D. Pham, J. Chang, M. A. Zurbuchen and J. P. Chang, *Chem. Mater.*, 2015, **27**, 7282-7288.
18. J. F. Mosselmans, P. D. Quinn, A. J. Dent, S. A. Cavill, S. D. Moreno, A. Peach, P. J. Leicester, S. J. Keylock, S. R. Gregory, K. D. Atkinson and J. R. Rosell, *J. Synchrotron Radiat.* , 2009, **16**, 818-824.
19. Y. Takahashi, T. Uruga, K. Suzuki, H. Tanida, Y. Terada and K. H. Hattori, *Geochim. Cosmochim. Acta*, 2007, **71**, 5180-5190.
20. Y. Takahashi, T. Uruga, H. Tanida, Y. Terada, S. i. Nakai and H. Shimizu, *Anal. Chim. Acta*, 2006, **558**, 332-336.
21. J.-H. Choy, D.-K. Kim and J.-Y. Kim, *Solid State Ion.*, 1998, **108**, 159-163.